Dynamic Response and Activation-timing Effects in Hybrid Shape Memory Alloy Semi-active Vehicle Suspensions

Ala'a Al-Falahat

Department of Mechanical Engineering, Faculty of Engineering, Mutah University, P.O Box 7, Al-Karak 61710, Jordan
Email: alaa.falahat@mutah.edu.jo

***Abstract*—This paper investigates the effect of activation time on the behavior of hybrid semi-active suspensions that incorporate Shape Memory Alloy (SMA) components with Magnetorheological (MR) damping or piezoelectric actuation. A two-degree-of-freedom quarter-car model is used to compare three configurations: passive + SMA, SMA + MR, and SMA + piezoelectric actuator when subjected to harmonic, stochastic, and bump-type road inputs. The model was implemented in Python and tested on the displacement of the sprung mass, acceleration of the sprung mass, Fast Fourier Transform (FFT) response, Root Mean Square (RMS) acceleration, deflection of the suspension, and tyre-load variation. Two activation strategies are considered: fixed-time engagement and threshold-based logic, which is triggered by the vibration level. The results show that activation time is not an additional design consideration; delayed activation increases peak response and settling time, particularly under transient disturbances. Within the present simulation framework, the SMA + piezoelectric layout provides the largest numerical reduction in body motion and acceleration, whereas the SMA + MR layout offers a more conservative balance between performance and implementation complexity. Frequency-domain results indicate lower resonance amplitudes for the two hybrid layouts than for the passive benchmark. Because the analysis is simulation-driven, the results should be interpreted as comparative trends rather than experimentally validated performance limits. The study clarifies design balance in hybrid smart suspensions and provides a repeatable platform for future experimental and hardware-in-the-loop validation.**

***Keywords*—hybrid semi-active suspension, shape memory alloy, magnetorheological damper, piezoelectric actuator, activation timing, vibration control**

I. Introduction

Vehicle-suspension research is progressing gradually from the passive fixed-tuned state to an adaptive and semi-active state that adapts to road conditions and vehicle state. More recent reviews and experimental investigations report on ongoing advances in control using Skyhook approaches [1–4] as well as on Magnetorheological (MR) damping and predictive quarter-car platforms [2, 4, 5] that allow for an improvement in ride comfort without the constant energy demand of full active suspension systems. Meanwhile, the piezoelectric devices are receiving renewed attention as high-bandwidth force-modulation elements, as well as Shape Memory Alloy (SMA) components, which are attractive due to their recoverable strain, compact packaging, and inherent hysteretic dissipation [6–10]. The developments highlight hybrid smart suspensions as a viable design approach for intelligent vehicles, not just a theoretical concept.

Practical implementation remains difficult. MR devices are fast and tunable, and highly nonlinear and current-dependent. Piezoelectric branches are stroke-limited, have high bandwidth, and are very sensitive to force and/or voltage. The value of recoverable and dissipative behaviours from SMA branches is useful; however, the process is slower as it relies on constitutive and thermal activation effects [2–10]. Most of the latest research still concentrates on a single actuator family or the ideal control engagement. Few studies have focused on the coordination of a slower SMA branch with faster semi-active or active components under activation delay, threshold logic and mixed road inputs.

This paper investigates the performance of the hybrid SMA-based suspension systems subject to actuator coordination and activation timing. The objective is to compare passive + SMA, SMA + MR and SMA + piezoelectric configurations in the same consistent quarter car model and to assess them with harmonically, stochastically and transiently applied vibrations, based on common ride-comfort and road-holding metrics.

The use of a numerical framework is also crucial as a pre-experimental stage, as it allows for the isolated investigation of the timing of SMA activation and the coordination of the hybrid-branch at the same quarter-car assumption. Before hardware testing, it can be used to determine which control variables are most sensitive, compare alternative hybrid designs based on common performance measures and minimize subsequent hardware-in-the-loop or prototype effort by concentrating on the most promising designs.

The paper contains four main contributions. Firstly, a unified numerical model is built in which the mechanical

Manuscript received April 2, 2026; revised May 14, 2026; accepted June 3, 2026; published August 17, 2026.

doi: 10.18178/ijmerr.15.4.423-432

baseline is kept, and the auxiliary smart branch is modified. Second, it introduces fixed-time and threshold-based SMA activation, allowing for the effect of delayed engagement to be investigated explicitly. Third, it examines three hybrid layouts based on three time- and frequency-domain, and metric-based ride-comfort responses. Finally, it interprets the results with caution by separating the peak vibration suppression, complexity of the control, realism of the actuators and limitations of the implementation.

The manuscript is structured as described below; Section II is a review of recent suspension studies and formulation of the research gap. In Section III, the model, the control logic, the choice of the different parameters and the assumptions for the simulation are presented. The numerical results are reported in Section IV, a discussion of the benchmarking and limitations is given in Section V, and the paper ends with conclusions and suggestions for future work in Section VI.

II. Literature Review

In recent publications, various approaches have been classified as MR damping, active or predictive control, SMA-based damping, and high-bandwidth piezoelectric actuation. The approaches of these recent publications can be divided into four main directions: MR damping, active or predictive control, SMA-based damping, and high-bandwidth piezoelectric actuation. Wang *et al.* [11] summarized automotive MR suspensions and pointed out that tunable damping and fast response were significant benefits, and that hysteresis modelling, inverse control, and controller robustness were significant challenges. This problem was partially solved by Yoon and Choi [12] through adaptive control of an MR damper for an in-wheel motor vehicle, where vibration attenuation capability was enhanced, but hybrid actuator coordination was not considered. Li *et al.* [13] achieved improved comfort and handling with the help of semi-active air suspension and MR damping using S-QFSMC control, but the result is that the controller is more complex and requires more accurate state information. The idea of semi-active suspension control comes from the pioneering work of Karnopp *et al.* [14], who first proposed controllable damping strategies that are the basis of modern semi-active systems.

A second group of studies has focused on optimal and coordinated active control. Abbas and Youn [15] employed an actuator-controlled aero-body with a quarter-car model and demonstrated that coordinated external force shaping can enhance the ride and road holding of the system. Zhao *et al.* [16] further extended the problem to combined active suspension and anti-lock braking control for electric vehicles, which further emphasized the necessity of cross-system coordination while also making the system more complex. Park *et al.* [17] proposed a rotary MR damper for a low-floor vehicle and tested it experimentally, revealing that the damping bandwidth can be influenced by the design of the damper as much as by the controller.

The third stream is also closely related to the current research work, since it investigates the damping of SMA in motor vehicles. Huang *et al.* [18] designed a rubber-based SMA composite damper based on multi-body dynamics and response surface methodology, which showed that the stiffness and damping of the composite damper were improved, especially for cab-vibration attenuation. In another study by Huang *et al.* [19], the effective stiffness and damping of rubber-SMA composite absorbers were proven to be highly sensitive to the loading rate. This outcome verifies that SMA-supported performance is a non-constant parameter phenomenon. However, these works give valuable component-level design information, not taking the hybrid suspension branches' activation time into account.

The fourth stream is related to fast electrical actuation and active control. Zhou *et al.* [20] have reviewed the piezoelectric actuators, noting that the characteristics of high bandwidth, precision, and compactness are desirable, but the small stroke and the need for amplification or force control are not. In the actual device, the timing variable is employed to investigate the effect of delayed engagement on the suspension response and the model is assumed to reflect such an effect. Haseen and Lakshmi [21] implemented an optimised Linear-Quadratic Regulator (LQR) on an active suspension and achieved a good degree of vibration suppression, but their conclusions also showed the well-known compromise between better ride metrics and higher controller loads. In the field of active suspension, Li *et al.* [22] proposed an active speed-dependent suspension Model Predictive Control (MPC) based on road-preview information, demonstrating that predictive inputs can enhance the damping decisions but involve extra sensing and estimation layers.

Recent works in the field of nonlinear control give additional insight into the state of the art. Diao *et al.* [23] designed a hierarchical controller for an uncertain active suspension with time-varying disturbances and demonstrated the effectiveness of force-tracking structures in terms of displacement and acceleration control in response to random and bump inputs. Zhao *et al.* [24] adopted a semi-active air suspension system involving an MR damping system with neural-network modelling, delay compensation, and adaptive backstepping to mitigate the effects of actuator delay and uncertain sprung mass. Bahar *et al.* [25] reviewed parametric MR-damper models and showed that control quality is highly sensitive to the ability of the model to represent inverse-damper behavior. Liu *et al.* [26] stated that the overall direction of the development of lightweight and smart suspensions for new-energy vehicle systems was being introduced, where intelligent damping is increasingly discussed alongside packaging, mass, and energy requirements.

A comparison of the present results with representative studies on suspensions in recent years is presented in Table I. Such comparison is not intended to establish that there are strict equivalences between different models and test conditions; rather, it puts into perspective that the trends described here moderate gains in semi-active MR control, stronger gains in faster active or pseudo-active branches, and an ongoing realist gap between implementation and theory, generally concurring with the trend of the recent literature [11–26].

TABLE I. SUMMARY OF RESEARCH GAPS IDENTIFIED FROM THE LITERATURE AND THE CONTRIBUTION OF THE PRESENT STUDY

Study type	Representative actuator	Method focus	Typical reported outcome	Main limitation
MR semi-active studies [11–13, 17, 25]	MR damper	Skyhook, adaptive, or semi-active nonlinear control	Improved damping authority and ride metrics	Hysteresis modelling and controller tuning remain demanding
Active/predictive studies [15, 16, 21–24]	Electro-hydraulic, active force, or predictive control	LQR, MPC, hierarchical or adaptive control	Stronger displacement and acceleration reduction	Higher complexity, sensing burden, or actuator effort
SMA composite studies [18, 19, 27–29]	SMA or SMA-based composite damper	Material design and reduced-order constitutive modelling	Higher damping and recoverable-force capability	Timing, thermal response, and full hysteresis remain challenging
Present study	SMA + MR / piezoelectric hybrid	Unified comparison with activation timing	10–21% response reduction depending on the metric	Simulation only; no full power or uncertainty model

Therefore, three gaps are evident from these studies. First, less frequented than fully active systems and pure MR systems are hybrid SMA-based suspensions. Second, activation timing is usually assumed to be ideal or instantaneous, but it could be delayed in smart-material branches. Third, in many studies, one architecture is optimized, and the contribution of coordination among passive, semi-active and active components cannot be distinguished. The current work addresses these gaps by applying one modelling framework to investigate the effectiveness of three hybrid layouts derived from SMA and by exploring the effect of activation timing on the effectiveness of the hybrid layouts.

III. METHODS

A. Quarter-Car Configuration and Coordinates

Three suspension layouts considered in this work are summarized in Fig. 1. The mechanical model in both cases is a two degree of freedom quarter car model: a sprung mass, denoted as m_s, and an unsprung mass, denoted as m_u. The sprung mass is the vehicle frame body, and the unsprung mass is the wheel/axle assembly. The passive + SMA system consists of a conventional spring-damper system and an SMA branch that provides recoverable force and hysteretic dissipation. The SMA + MR configuration uses a controllable MR damper in parallel with the passive and SMA elements. The SMA + piezoelectric configuration uses an actively commanded piezoelectric actuator in place of the semi-active branch.

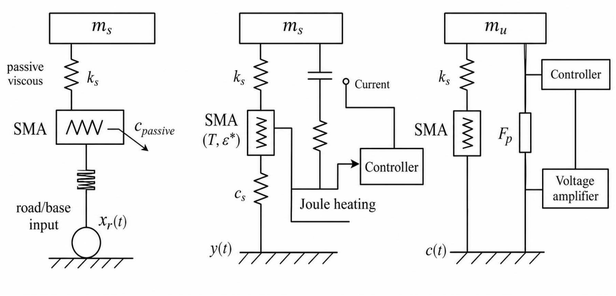

(a) (b) (c)

Fig. 1. Hybrid SMA suspension configurations used in the quarter-car model: (a) passive + SMA, (b) SMA + magnetorheological damper, and (c) SMA + piezoelectric actuator.

The generalized coordinates are the displacement of the sprung mass, $x_{s(t)}$, the displacement of the unsprung mass, $x_{u(t)}$ and the displacement of the road, $x_{r(t)}$. The linear spring k_s and the passive damper $c_{passive}$ are suspended between the two masses, and the smart branch is provided for the selected configuration. Stiffness k_t and optional damping c_t of the tyre are assumed.

Define the relative suspension deformation, $y(t) = x_{s(t)} - x_{u(t)}$ and the relative velocity, $\dot{y} = \dot{x}_s - \dot{x}_u$.

Although a higher-order full-vehicle model can capture pitch, roll, axle coupling, suspension geometry, and tyre-relaxation effects, the quarter-car model remains a widely used benchmark for vertical ride analysis and controller comparison. Its primary advantage is the transparency, as the contribution of each branch of the damping or of the actuation can be isolated, without the additional degrees of freedom obscuring the influence. Also, it is important to note that it is limited and should not be used for full-vehicle prediction but rather as trends in vertical dynamics.

B. Equations of Motion

Suppose the transmitted force through the suspension path is $F_{susp(t)}$, taken as positive upward on the unsprung mass. Eqs. (1) and (2) give the coupled equations of motion.

$$m_s\ddot{x}_s = -F_{susp} \tag{1}$$

$$m_u\ddot{x}_u = F_{susp} - k_t(x_u - x_r) - c_t(\dot{x}_s - \dot{x}_u) \tag{2}$$

where $c_t = 0$ when tyre damping is neglected.

The total suspension force is the sum of the parallel spring, passive damping, SMA, and auxiliary control branches, as written in Eq. (3).

$$F_{susp} = k_s\,y + c(t)\,\dot{y} + F_{SMA,rec}(y,z,T) + F_{MR}(u_{MR},\dot{y}) + F_{piezo}(u_{pz},e,\dot{e}) \tag{3}$$

C. Passive + SMA Equivalent Damping and Activation Logic

The combined passive and SMA dissipation is represented through the equivalent damping expression in Eq. (4).

$$c(t) = c_{passive} + c_{SMA}(t) \tag{4}$$

The activation law is introduced in piecewise form in Eq. (5), so that the SMA contribution changes only after engagement.

$$c_{SMA}(t) = \begin{cases} c_{SMA,0} & t < t_{act} \\ c_{SMA,0} + \Delta c_{SMA} & t \geq t_{act} \end{cases} \quad (5)$$

Here, t_{act} is the activation time. In practical terms, this timing represents a simplified form of thermal triggering or logic-based engagement. The model assumes that in a real device, the timing variable is used to study the influence of delayed engagement on the suspension response.

The energy-equivalent viscous damping is approximated using the area of the SMA force-displacement loop for near-harmonic motion, based on Eq. (6).

$$c_{SMA,eq} = \frac{\Delta E_{SMA}}{2\,\pi\,\omega\,Y^2} \quad (6)$$

using the loop area of the ΔE_{SMA} force–displacement cycle; for transients, compute $c_{SMA}(t)$ over a short sliding window. In transient cases, the equivalent damping is estimated on a relatively short sliding window, in order to preserve the response dependency of the dissipation estimate while keeping it away from the pure steady-state.

The SMA branch is also switched on by a threshold rule to capture the practical semi-active logic. This formulation is triggered when the body acceleration recorded in the test or the suspension deformation is above a certain level. This rule is not meant to be a fixed switching time but a decision rule based on the sensor.

$$\text{Activate SMA if: } \ddot{x}_s(t) \geq a_{th} \text{ or } x_s(t) - x_u(t) \geq \delta_{th}$$

where a_{th} and δ_{th} are the acceleration and displacement thresholds, respectively. Once activated, the SMA branch adds hysteretic damping to the response until the response drops below the threshold. This implementation assumes ideal threshold measurements, which include sensor noise, filtering and controller latency, are discussed as limitations later and are not fully simulated in the present study.

D. SMA Recoverable (Self-Centring) Force

The recoverable SMA force is modelled as a simplified bilinear superelastic model (Eq. (7)). This reduced order form is often employed when the full thermomechanical constitutive integration is not possible [27, 29].

$$F_{SMA,rec} = \begin{cases} k_A\,y & |y| \leq y_y \\ k_A\,y_y\,sgn(y) + k_P\,(y - sgn(y)y_y) & |y| \leq y_y \end{cases} \quad (7)$$

The recoverable branch of this expression is given by the austenite stiffness k_A, the post-plateau stiffness k_P and the transformation, the dissipative effect $c_{SMA}(t)$ is retained by the equivalent damping term in Eq. (4).

E. SMA + MR Damper (Dual-Mode)

Two types of standard MR representation are considered: the variable-viscosity model and the Bingham-type model with controllable yield stress, as given by Eqs. (8) and (9).

(I) Variable-viscosity model:

$$F_{MR} = c_{MR}(u_{MR})\,\dot{y} \quad (8)$$

(II) Bingham model with controllable yield:

$$F_{MR} = c_{MR}(u_{MR})\,\dot{y} + f_y(u_{MR})\,sgn(\dot{y}) \quad (9)$$

The control command I (coil current/voltage) controls the level of cMR damping and, if applicable, the yield force. It is observed that the MR branch is reactive, and the SMA branch follows the activation law from Eq. (5). This separation enables the faster MR element to make up for some of the missed SMA engagement.

A classical Skyhook rule is used to calculate the MR damping coefficient, so that it increases when the velocity of the sprung mass requires energy to be dissipated and decreases otherwise [1, 11, 12]. This rule ensures that the semi-active force is physically realisable and has a simple controller architecture.

F. SMA + Piezoelectric Actuator (Active–Passive Hybrid)

The piezoelectric actuator provides an active control force in the suspension path. If the target is set to $r = 0$, then the commanded force is defined by Eq. (10).

$$F_{piezo} = K_p e + K_d\,\dot{e},\; e = r - y \quad (10)$$

The controller is very simple and uses Proportional-Derivative (PD) feedback because piezoelectric devices are high bandwidth, but stroke-limited. This selection eliminates the need to implement a highly optimized control law and reduces the improvement to that due to the application of the force at high speed.

Piezoelectric force saturation is explicitly enforced to keep the simulation physically realistic.

$$|F_{piezo}| \leq F_{max}$$

F_{max} is the saturation force that is achievable based on practical voltage and material limits. Hence, the SMA + piezoelectric results should be considered in terms of limited, rather than unlimited, actuator behaviour [20, 28].

The SMA actuator is not only triggered according to a fixed timing, but also depending on measured dynamic conditions. The MR damper works on a Skyhook control strategy, and the max actuator force is limited by saturation constraints, reflecting the realistic capability of the actuator.

To clarify the implementation sequence of the proposed hybrid SMA suspension simulation, the overall computational workflow is summarized in Fig. 2. This figure shows the flow from road excitation, calculation of quarter-car dynamic response, to activation via the sensors, selection of the auxiliary branch, calculation of total suspension force, and extraction of performance metrics.

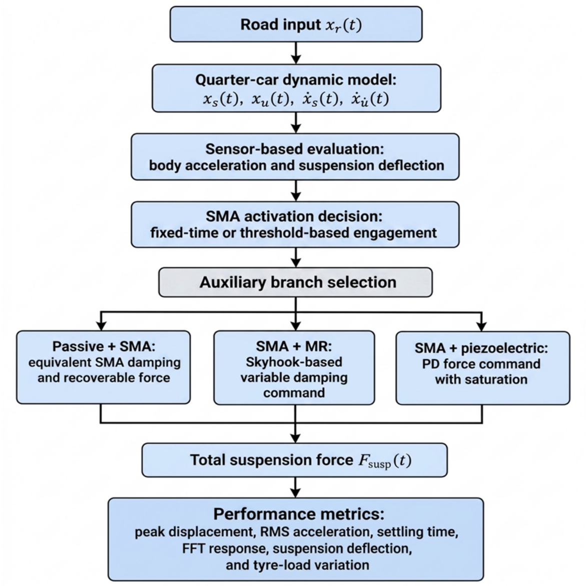

Fig. 2. Schematic control flow of the hybrid SMA suspension simulation.

G. State-Space form for Simulation

Combining Eqs. (1)–(3) gives the compact state-space form used for numerical integration and controller implementation.

$$m_s\ddot{x}_s + m_u\ddot{x}_u = k_t(x_u - x_r) - c_t(\dot{x}_s - \dot{x}_u), \ddot{y} = \ddot{x}_s - \ddot{x}_u \tag{11}$$

Substituting the force balance into Eqs. (1) and (2) gives the state equations in Eqs. (12) and (13).

$$m_s\ddot{x}_s = -k_s\, y - c(t)\dot{y} - F_{SMA,rec} - F_{MR} - F_{piezo} \tag{12}$$

$$m_u\ddot{x}_u = k_s y + c(t)\dot{y} + F_{SMA,rec} + F_{MR} + F_{piezo} - k_t(x_u - x_r) - c_t(\dot{x}_u - \dot{x}_r) \tag{13}$$

H. Simulation Setup and Excitation Inputs

The model is simulated first with sinusoidal base excitation $x_{r(t)}$ = A sin($2\pi ft$), where amplitude A = 0.1 m and frequency f = 1 Hz. These values are maintained from the original study as they excite the dominant low-frequency ride mode and enable direct comparison between the three hybrid layouts.

Sprung and unsprung masses: m_s = 250 kg and m_u = 40 kg.

- Suspension stiffness and damping: k_s = 15 kN/m and $c_{passive}$ = 1000 N·s/m.
- Tyre stiffness and damping: k_t = 200 kN/m and c_t = 0 N·s/m; the tyre damping is neglected for the baseline simulations.
- SMA dissipation: $c_{SMA(t)}$ is determined using energy-equivalent damping from the SMA loop area at the selected amplitude and frequency. Before activation, c_{SMA} = 0. Once activated, $c_{SMA} = 0 + \Delta c_{SMA}$, where Δc_{SMA} = 3000 N·s/m. The baseline activation time t_{act} is set at 1 s, and the sensitivity for 0.5, 1.5, and 2.0 s are investigated.

All simulations are run from zero displacement and velocity unless otherwise specified. The integration time is 5 s, long enough to capture activation, transient decay, and the post-activation oscillation envelope.

A stochastic road profile is used to assess robustness under more realistic operating conditions in addition to sinusoidal excitation. The movement of the road is represented by a filtered white-noise process according to the ISO 8608 road-roughness classification. This excitation is a random noise from road irregularities, and the ride-comfort and road-holding trends can be measured independently of harmonic excitation. These trends in robustness are investigated in the stochastic case, and hence only the overall trends in the numerical performance are presented, but detailed time histories are therefore omitted for brevity. The transient road disturbance is also applied as a single half-sine bump input. This is an excitation to measure the response of the suspension to sudden disturbances like a track joint, a pothole or a rail switch.

To evaluate ride comfort and safety quantitatively, the following performance indices are computed:

1) RMS sprung-mass acceleration (a_rms), which is widely used as a ride-comfort indicator according to ISO 2631.

2) Maximum suspension deflection, $|x_s - x_u|$max, which represents suspension stroke limitation.

3) Dynamic tyre-load variation, defined as the standard deviation of the tyre force, which indicates road-holding capability.

These metrics provide an objective comparison among suspension configurations beyond qualitative inspection of time histories.

I. Parameter Selection, Benchmarking Context, and Assumptions

The selected mass, stiffness, and damping values are literature-consistent quarter-car baseline values and are not experimentally identified values for a specific production vehicle. They are nevertheless of the same order of magnitude as recent quarter-car, MR-damper, and pseudo-active suspension experiments, allowing the relative results to be interpreted physically even though the present model is not hardware identified [9, 11, 17, 29].

A global sensitivity analysis and statistical uncertainty assessment are out of scope of the present revision. Accordingly, the manuscript interprets the numerical improvement as relative trends obtained under modelling assumptions. This clarification is important because the object of this study is not to establish a universally optimal parameter set, but rather to isolate the effect of SMA activation timing and branch coordination on response quality within a repeatable simulation framework.

IV. Results

A. Baseline System Response

1) Sprung mass displacement

Fig. 3 shows the comparison of the displacement of the passive system and the passive + SMA system.

Before activation, the two traces are almost the same since the SMA branch has not yet increased effective damping. At t = 1.0 s, the SMA-assisted envelope moves more rapidly, which means that the body gets closer to equilibrium with less sustained vibration.

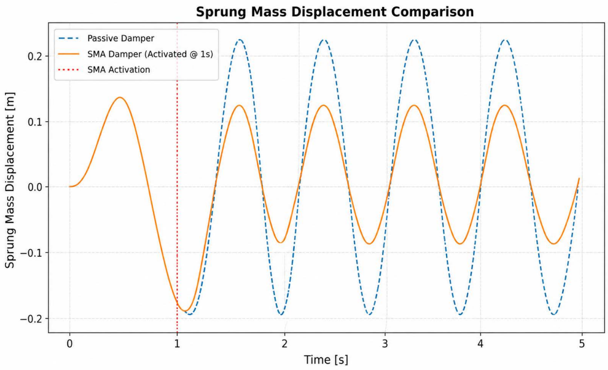

Fig. 3. Sprung-mass displacement for the passive system and the passive + SMA system with activation at t = 1.0 s.

Once activated, the envelope of the passive response continues to oscillate with a relatively wide envelope, while the activated SMA envelope is more in the region of ± 0.12 m. This confirms the purpose of the SMA branch: it will add dissipation when it is engaged without needing to have a continuously powered actuator. The benefit, however, is highly dependent on the timely engagement, as shown in Sections IV.D and IV.E.

2) Sprung mass acceleration

Fig. 4 shows representative sprung-mass accelerations. Smoothing the response at each instant will not be expected when damping is increased because sharper corrective forces will be transmitted. The important observation is the reduction of the acceleration envelope after the switching event.

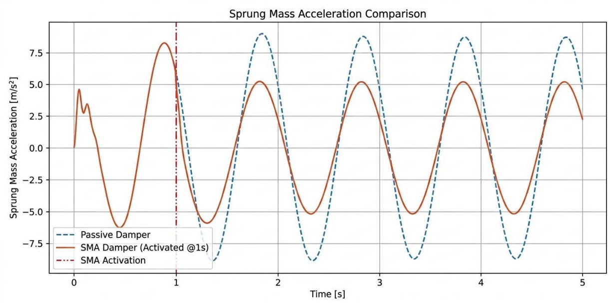

Fig. 4. Sprung-mass acceleration for the passive system and the passive + SMA system with activation at t = 1.0 s.

The peaks of the passive damper response are sustained at around ±8.5 m/s^2, while the peaks of the SMA-assisted damper response are reduced to approximately ±5 m/s^2 towards the latter part of the record. The activated SMA branch not only decreases the displacement but also the time for which the vehicle body is subjected to repeated peak acceleration from a ride-comfort point of view. The compromise is that larger corrective forces may be transferred for a brief time if the damping is increased.

B. Hybrid Suspension Response

Before activation, the three hybrid configurations are similar in their response since the auxiliary branches are inactive or weakly active. The differences in the results can be seen at t = 1.0 s, when the additional smart branch starts to affect the sprung-mass motion.

Fig. 5 shows that the passive + SMA case has the largest displacement envelope, the SMA + MR case provides a smaller envelope, and the SMA + piezoelectric case gives the smallest excursion. As shown in Table I, the positive and negative displacement peaks with the SMA + MR arrangement are reduced from +0.14 m and −0.16 m to +0.12 m and −0.14 m, respectively, after the post-activation. The peaks are further reduced to +0.11 m and −0.13 m using SMA + piezoelectric layout. The MR branch is activated to add damping authority without the complete change to active control, while the Piezoelectric branch provides an extra corrective quick response force. These gains for the SMA + piezoelectric layout should therefore be treated with caution: not only does a gain exist for the active feedback path, but the saturation condition in Section III.F still applies to the SMA branch. Therefore, the configuration should be regarded more as the high-performance case of this present numerical study than as a production-ready configuration.

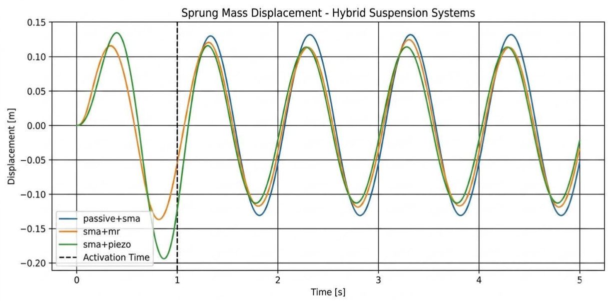

Fig. 5. Sprung-mass displacement of the three hybrid suspension configurations with activation at t = 1.0 s.

TABLE II. COMPARISON OF PEAK SPRUNG MASS DISPLACEMENTS FOR HYBRID SUSPENSION SYSTEMS

System	Positive Peak (m)	Negative Peak (m)	% Reduction (Positive) vs Passive + SMA	% Reduction (Negative) vs Passive + SMA
Passive + SMA	+0.14	–0.16	–	–
SMA +MR	+0.12	–0.14	~15%	~12.5%
SMA + Piezo	+0.11	–0.13	~21%	~19%

The result of the displacement comparison is summarized in Table II in a benchmark-friendly format. It shows that whether semi-active or piezoelectric, both hybrid branches give an improvement of the post-activation response compared to passive + SMA, but in different ways: active + SMA provides the semi-active damping authority, whereas passive + piezoelectric provides the bounded active correction. This is important because of the distinction for design selection. In cases where moderate complexity and conservative semi-active implementation are preferred, the MR branch may be used, while in cases where the application demands a more powerful body-motion control, the piezoelectric branch may be used for its greater complexity.

Fig. 6 shows the acceleration responses of the three configurations. Again, the largest residual oscillation after activation is the passive + SMA. The peaks are reduced in the SMA + MR case, and the SMA + piezoelectric case gives the smoothest decay of the three cases.

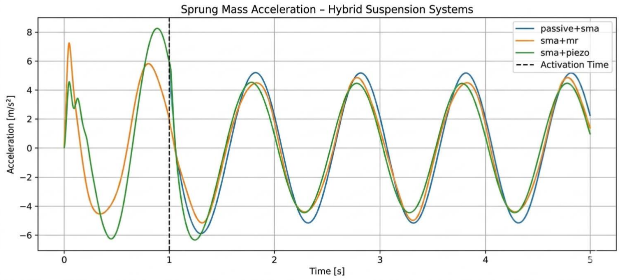

Fig. 6. Sprung-mass acceleration of the three hybrid suspension configurations with activation at $t = 1.0$ s.

As presented in Table III, the +SMA and +SMA + MR configurations are very similar in terms of the positive acceleration peak (+5.0 m/s² and +4.8 m/s² respectively), and SMA + Piezo is nearly equal to −0.5 m/s². The negative side is a decrease in the peak from −5.5 m/s² to −5.0 m/s² and −4.8 m/s², respectively. These reductions are less than the displacement reductions, showing that it will be easier to achieve body-motion suppression than uniform acceleration reduction as the damping becomes more aggressive.

TABLE III. PEAK SPRUNG-MASS ACCELERATIONS FOR THE HYBRID SUSPENSION SYSTEMS

System	Positive Peak (m/s²)	Negative Peak (m/s²)	% Reduction (Positive) vs Passive + SMA	% Reduction (Negative) vs Passive + SMA
Passive + SMA	+5.0	–5.5	–	–
SMA + MR	+4.8	–5.0	~4%	~9%
SMA + Piezo	+4.5	–4.8	~10%	~13%

Despite this difference, the ranking remains unchanged: SMA + piezoelectric gives the largest numerical acceleration suppression, while SMA + MR provides the stronger semi-active compromise. The consistency of this ranking in both displacement and acceleration responses suggests that the observed advantage is not limited to a single response variable.

C. *Frequency Analysis Using Fast Fourier Transform (FFT)*

The Fast Fourier Transform (FFT) of the sprung-mass acceleration is used to complement the time-domain results. As expected for the low-frequency ride mode of the chosen quarter-car parameters, all three hybrid layouts exhibit a strong resonance near 1.2 Hz, as displayed in Fig. 7. The highest normalized peak amplitude is found in the case of passive + SMA with a normalized peak value of ~5.2, while the SMA + MR and SMA + piezoelectric cases have normalized peaks of ~4.6 and ~4.5, respectively.

The interpretation can be separated into two frequency ranges. The dominant body mode is suppressed by the hybrid branches, and hence, smaller envelopes are obtained in the time domain near resonance. The amplitude is significantly reduced above about 2 Hz for all setups, with MR and piezoelectric slightly lower than passive + SMA. The MR branch has more damping effect, and the piezoelectric branch has the lowest dominant peak, but is more affected by the actuator authority and saturation limits.

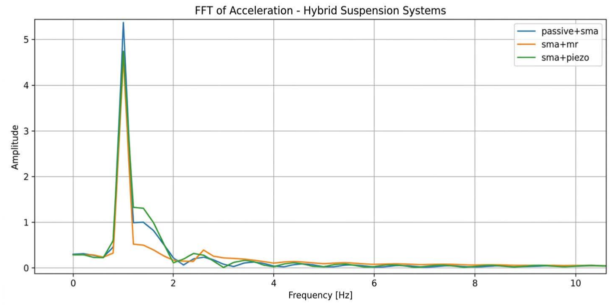

Fig. 7. Fast Fourier transform of sprung-mass acceleration for the three hybrid suspension configurations.

This frequency domain perspective also supports the emphasis of this study on coordination and not simply on raw actuator power. Near resonance, a faster branch may offer protection to the system, but the SMA contribution is delayed, and the benefit is dependent on the simplicity of the controller, the actuator capabilities, and the realistic implementation.

D. *Effect of SMA Activation Timing*

Table IV shows the effect of activation time on three performance indices: maximum displacement, RMS acceleration and settling time. The earlier the activation, the better the response. The lowest RMS acceleration of 3.51 m/s² and the shortest settling time of 1.8 s are at t_{act} = 0.5 s. Delaying activation to 2.0 s increases RMS acceleration to 4.40 m/s² and settling time to 2.9 s.

TABLE IV. SMA ACTIVATION TIMING VERSUS PERFORMANCE METRICS

Activation Time (s)	Max Displacement (m)	RMS Acc. (m/s²)	Settling Time (s)
0.5	0.045	3.51	1.8
1.0 (baseline)	0.050	3.77	2.1
1.5	0.056	4.12	2.6
2.0	0.062	4.40	2.9

E. *Control Logic Delay Effect Analysis*

The same trend is shown in Fig. 8 and Table V using peak-response values. Activation at 0.5 s keeps the maximum acceleration near ±5.5 m/s² and the maximum displacement near ±0.15 m. When activation is delayed to 1.0 s, 1.5 s, and 2.0 s, the peaks increase progressively. The 2.0 s case is substantially worse than the early-activation baseline.

The practical consequence is direct: delayed activation is not a cosmetic issue in a hybrid smart suspension. It changes the amplitude that the controller must subsequently reduce and therefore affects comfort and structural demand. For this reason, activation logic should be treated as a design variable rather than as an add-on.

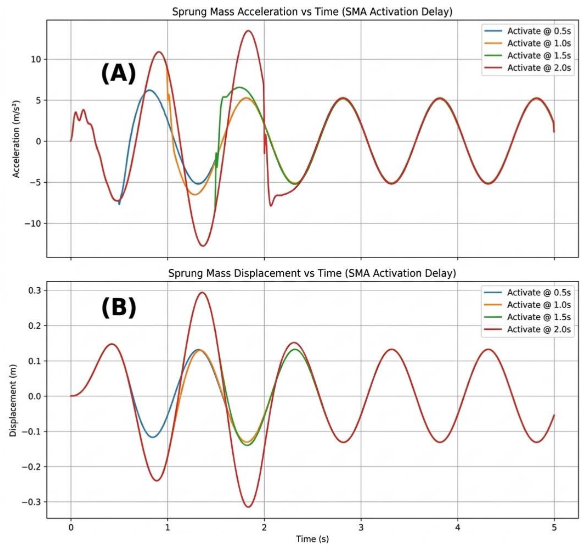

Fig. 8. Effect of SMA activation delay on sprung-mass dynamics: (a) acceleration response and (b) displacement response for activation times of 0.5 s, 1.0 s, 1.5 s, and 2.0 s.

TABLE V. EFFECT OF SMA ACTIVATION DELAY ON PEAK RESPONSES

Activation Time	Peak Acceleration (m/s²)	% Increase vs 0.5 s	Peak Displacement (m)	% Increase vs 0.5 s
0.5 s	±5.5	–	±0.15	–
1.0 s	±7.0	~27%	±0.20	~33%
1.5 s	±9.0	~63%	±0.23	~53%
2.0 s	±12.5	~127%	±0.30	~100%

V. DISCUSSION

The results show that the hybridization process has a positive impact on the quarter-car response, which varies according to the hybridization configuration. The passive + SMA layout also has an additional contribution of dissipation after activation, but with a somewhat slower contribution from the SMA branch. The SMA + MR layout improves the response by combining the SMA branch with a semi-active damper for faster response. The SMA + piezoelectric layout is further enhanced by introducing a bounded active force; hence, it is found to produce the lowest displacement and acceleration peaks in the current numerical framework. It's also the least conservative architecture in terms of implementation.

The frequency domain interpretation is consistent with the time domain interpretation. Both hybrid branches offer a decrease in the dominant low-frequency resonance, the frequency region most important to ride comfort for the present model. The SMA + MR case is significant because it helps lower the resonance peak without having to implement an energy-hungry strategy all the time. The SMA + piezoelectric case gives the best numerical values, but this improvement is linked to controller bandwidth and force saturation rather than to SMA hysteresis alone.

The most important cross-cutting outcome is the use of activation timing. Lower RMS acceleration, settling time and peak displacement when exposed to transient disturbance at earlier engagement. So, the hybrid branch is best when it is activated before the movement of the body becomes large. For SMA designs, this is the most relevant, since the benefit of the material will be diminished if the triggering electronics are slow or the thermal response is slow.

In both cases, the stochastic and bump inputs have the same qualitative interpretation. Under less periodic excitation, it does not change the ranking found under harmonic excitation, but it demonstrates how significant the timing and branch coordination are under less periodic excitation. This supports the idea that there is as much need for controller coordination as there is for material selection.

In the engineering design sense, the three designs represent different priorities. Passive + SMA is a basic solution to the standard suspension. SMA + MR is a moderate complexity semi-active compromise. SMA + piezoelectric is the strongest numerically, but the benefit of this combination depends on the availability of a bounded active branch that can provide fast and repeatable force output with minimal power consumption and without causing any degradation of output due to saturation.

This is because percentage improvements should be interpreted within the context of these differences. The displacement reduction is desirable, but must be matched with the complexity of the control, the realism of the actuators and the uncertainty of the simplified constitutive laws. The paper's contribution is not just to establish the optimal numerical layout but also to understand the mechanism of each improvement.

The revision expands the limitations discussion so that the claims remain consistent with what the model can support. The key constraints are as follows.

1. Reduced-order vehicle model: the two-degree-of-freedom quarter-car model only accounts for the vertical dynamics of the ride but cannot represent pitch, axle coupling, tyre relaxation, and suspension-geometry effects.
2. Simplified SMA representation: the SMA branch is represented by equivalent damping and a simplified bilinear recoverable-force law. The model thus does not explicitly deal with temperature evolution, temperature hysteresis or cycle dependence [27, 29].
3. Limited actuator realism: the MR and piezoelectric branches include control logic and saturation, but not detailed magnetic hysteresis, driver electronics, temperature drift, sensor noise or explicit controller latency. Therefore, the threshold logic should not be interpreted as an implementation model that is completely instrumented, but instead as a clean number baseline.
4. No dedicated power model: This paper describes the complexity of the control and its likely energy consumption, but does not provide a dedicated model of the amount of power consumed. For this reason, claims about real-world applicability are stated cautiously.
5. No statistical uncertainty analysis: The gains reported are deterministic results obtained from one numerical model. It should be interpreted as comparative tendencies under the stated assumptions rather than as statistically generalized performance limits.

Even with these restrictions, the model is useful for a reproducible comparison tool. Future experiments would be more feasible if quarter-car experiments were performed using displacement sensors, accelerometers, and controllable MR/ piezoelectric equipment to validate the activation logic by comparing it with the measured actuator behavior of a quarter car [9, 10, 17].

A hardware-in-the-loop test is a viable step between simulation and full prototype development. This configuration would allow for the performance of the quarter-car dynamics in real time with measured forces supplied by physical actuators and be able to test delayed activation, saturation, and controller time delays under controlled laboratory conditions [9, 10].

Further studies should integrate additional road classifications, parameter-identification experiments, and actuator-in-use data to assess the general trends in numerical coordination reported here in more challenging operating scenarios.

The overall methodology of the current study is consistent with the author's earlier research that involved rotor-dynamic modelling, unbalance behaviour and balancing strategies in the study of vibrating rotating mechanical systems [30–32]. Furthermore, the author's latest investigations in material-performance analysis and physics-informed engineering interpretations of material behaviour also highlight the significance of the material behaviour-mechanical performance relationship at a system level, applicable also to the discussion of smart suspension design in this paper [33, 34].

To summarise, the passive + SMA layout is the least complicated to improve post-activation, yet is most sensitive to activation delay. In the layout SMA + MR, post-activation displacement peaks are reduced by about 15% on the positive side and 12.5% on the negative side compared to passive + SMA; acceleration peaks are reduced by about 4% and 9%, respectively. The SMA + piezoelectric layout provides the greatest numerical suppression, with displacement reductions of ~21% and ~19% and acceleration reductions of ~10% and ~13%. The result also shows that the amplitude of the dominant resonance is smaller for SMA + MR and SMA + piezoelectric than for passive + SMA in the frequency domain. Thus, SMA + MR is the conservative semi-active choice, while SMA + piezoelectric is the top performance choice, under the assumptions and saturation limits of the present simulation.

VI. Conclusion and Future Work

This paper introduced a common numerical analysis of hybrid SMA suspension layouts in a quarter-car benchmark. Hybridization enhanced the response over the passive baseline in the tested cases, but the source of enhancement was heavily contingent upon the method and timing of activation and coordination of the auxiliary branch.

The most important result is that the timing of activation is significant in the performance of suspension. Early activation helps lower RMS acceleration, peak response, and settling time, while delayed activation leads to growing oscillations, which will then hinder the smart branch's ability to act effectively. Activation logic should therefore be considered a design variable, similar to stiffness, damping, and control gain.

The SMA + piezoelectric layout achieved the greatest numerical suppression of displacement and acceleration, the SMA + MR layout gave the best compromise between performance increase and complexity of control, and the SMA + electromagnetic hybrid achieved the lowest level of suppression of displacement and acceleration. The passive + SMA case showed the best improvement in response following activation and had the largest sensitivity to delay in activation.

From a practical design standpoint, the outcomes suggest that SMA elements could be employed as an additional damping branch if compactness and passive fail-safe behaviour are desired, whereas the SMA + MR configuration would be more appropriate for a realistic semi-active suspension design where moderate performance improvement is required but the active-force demand is not constant. For high-performance smart suspensions which allow for quick force correction and have adequate electrical authority, the SMA + piezoelectric configuration is most applicable.

Hence, the suggested numerical solution can be employed to select the hybrid smart-suspension layouts in the early stage of the design process prior to hardware-in-the-loop validation and thorough vehicle testing.

It should be noted that the reported percentage increases are not considered actual increases in performance in the real world, but rather as relative tendencies within the framework of the same model. These gains are nevertheless presented in an appropriate benchmarking context, and a realistic path to experimental/ hardware-in-the-loop validation is outlined.

Conflict of Interest

The author declares no conflict of interest.

Data Availability

The numerical data supporting the findings of this study are available from the corresponding author upon reasonable request.

References

[1] J. Wang, Z. Huang, H. Hong, S. Yu, W. Shi, and X. Zhang, "Skyhook-based techniques for vehicle suspension control: A review of the state of the art," *Machines*, vol. 13, no. 8, 727, 2025. doi: 10.3390/machines13080727

[2] A. A. Ferhath, "Vehicle performance enhancement through magnetorheological dampers and machine learning integration," *Discover Applied Sciences*, vol. 7, 1234, 2025. doi: 10.1007/s42452-025-1234-x

[3] J. Lee and K. Oh, "Hybrid damping mode MR damper: Development and experimental validation with semi-active control," *Machines*, vol. 13, no. 5, 435, 2025. doi: 10.3390/machines13050435

[4] W. Tao, B. Chen, L. Zhou, Z. Zheng, J. Wu, and M. Duan, "Design of a magnetorheological suspension damper for an agricultural tractor seat based on adaptive neuro-fuzzy inference system and active disturbance rejection control," *Mechanical Sciences*, vol. 16, pp. 113–124, 2025. doi: 10.5194/ms-16-113-2025

[5] L. Knap, C. Graczykowski, and J. Holnicki-Szulc, "Vehicle vibration reduction using hydraulic dampers with piezoelectric valves," *Sensors*, vol. 25, no. 4, 1156, 2025. doi: 10.3390/s25041156
[6] Z. P. Wu and H. Wang, "Investigation of fatigue life and active vibration control via piezoelectric elements in vehicle suspension," *Scientific Reports*, vol. 15, 35971, 2025. doi: 10.1038/s41598-025-35971-y
[7] M. I. Hossain, M. S. Rabbi, and T. M. Ali, "Shape memory alloys in modern engineering: Progress, problems, and prospects," *RSC Advances*, vol. 15, pp. 33046–33100, 2025. doi: 10.1039/D5RA33046K
[8] H. M. Diep, Z. Z. H. Le, T. B. Diep, and Q. H. Nguyen, "Development and performance validation of a magnetorheological damper for passenger cars featuring a ball screw and MR brake," *Actuators*, vol. 15, no. 1, 17, 2026. https://doi.org/10.3390/act15010017
[9] C. Li, W. Qiu, W. Li, D. Tan, L. Qian, and X. F. Bai, "Design and experimental validation of a quarter-car pseudo-active suspension for body-on-frame vehicles," *Actuators*, vol. 15, no. 3, 142, 2026. doi: 10.3390/act15030142
[10] F. Al-Momani, M. Salah, and S. Nabhan, "Experimental evaluation of ride comfort for a quarter-car active suspension system using model-free control techniques," *Systems Science & Control Engineering*, vol. 14, no. 1, 2026. doi: 10.1080/21642583.2026.2164321
[11] Z. Wang, C. Liu, X. Zheng, L. Zhao, and Y. Qiu, "Advancements in semi-active automotive suspension systems with magnetorheological dampers: A review," *Applied Sciences*, vol. 14, no. 17, 7866, 2024. doi: 10.3390/app14177866
[12] D. S. Yoon and S. B. Choi, "Adaptive control for suspension system of in-wheel motor vehicle with magnetorheological damper," *Machines*, vol. 12, no. 7, 433, 2024. doi: 10.3390/machines12070433
[13] G. Li, Y. Gan, Q. Liu, H. Xu, D. Chen, L. Zhong, J. Deng, and G. Hu, "Performance analysis of vehicle magnetorheological semi-active air suspension based on S-QFSMC control," *Frontiers in Materials*, vol. 11, 1358319, 2024. doi: 10.3389/fmats.2024.1358319
[14] D. Karnopp, M. J. Crosby, and R. A. Harwood, "Vibration control using semi-active force generators," *Journal of Engineering for Industry*, vol. 96, no. 2, pp. 619–626, 1974. https://doi.org/10.1115/1.3438373
[15] S. B. Abbas and I. Youn, "Optimal control of a semi-active suspension system collaborated by an active aerodynamic surface based on a quarter-car model," *Electronics*, vol. 13, no. 19, 3884, 2024. doi: 10.3390/electronics13193884
[16] Z. Zhao, L. Zhang, X. Ding, Z. Zhang, S. Li, and L. Gu, "Integrated active suspension and anti-lock braking control for four-wheel-independent-drive electric vehicles," *Chinese Journal of Mechanical Engineering*, vol. 37, 20, 2024. doi: 10.1186/s10033-024-00998-x
[17] Y. J. Park, B. H. Kang, and S. B. Choi, "A new rotary magnetorheological damper for a semi-active suspension system of low-floor vehicles," *Actuators,* vol. 13, no. 4, 155, 2024. doi: 10.3390/act13040155
[18] Y. Huang, Q. Fan, Zhang H, L. Shao, and Y. Shi, "Optimization of dynamic characteristics of rubber-based SMA composite dampers using multi-body dynamics and response surface methodology," *Applied Sciences*, vol. 14, no. 21, 10063, 2024. doi: 10.3390/app142110063
[19] Y. Huang and H. Zhang, "The stiffness and damping characteristics of a rubber-based SMA composite shock absorber with a hyper-elastic SMA-constitutive model considering the loading rate," *Materials*, vol. 17, no. 16, 4076, 2024. doi: 10.3390/ma17164076
[20] X. Zhou, S. Wu, and X. Wang, "Review on piezoelectric actuators: Materials, classifications, applications, and recent trends," *Frontiers of Mechanical Engineering*, vol. 19, 6, 2024. doi: 10.1007/s11465-024-0006-x
[21] S. F. Haseen and P. Lakshmi, "Active suspension control using novel HB3C optimized LQR controller for vibration suppression and ride comfort enhancement," *Journal of Vibration and Control*, vol. 31, no. 13–14, pp. 2606–2623, 2025. doi: 10.1177/10775463241234567
[22] Q. Li, Z. Chen, H. Song, and Y. Dong, "Model predictive control for speed-dependent active suspension system with road preview information," *Sensors*, vol. 24, no. 7, 2255, 2024. doi: 10.3390/s24072255
[23] S. Diao, X. Zhao, D. Zhao, Z. Dong, and Y. Qin, "Hierarchical control of vehicle active suspension system with uncertain sprung mass and time-varying disturbance," in *Proc. the Institution of Mechanical Engineers, Part D: Journal of Automobile Engineering*, 2026, vol. 240, no. 4, pp. 1651–1665. doi: 10.1177/09544070251123456
[24] R. Zhao, W. Huang, and H. Xie, "Adaptive neural network backstepping control for the magnetorheological semi-active air suspension system with uncertain mass and time-varying input delay," *Journal of Vibration and Control*, vol. 32, no. 3–4, pp. 396–411, 2026. doi: 10.1177/10775463251123456
[25] A. Bahar, F. Pozo, M. Rashidi Meybodi, and S. Karami, "Magnetorheological fluid dampers: A close look at efficient parametric models," *Structural Control and Health Monitoring*, vol. 2024, 6860185, 2024. doi: 10.1155/2024/6860185
[26] Y. Liu, S. Wang, and J. Tan, "A review of the lightweight and smart McPherson suspension for new-energy vehicles," *Frontiers in Mechanical Engineering*, vol. 12, 1787696, 2026. doi: 10.3389/fmech.2026.1787696
[27] D. C. Lagoudas, *Shape Memory Alloys: Modeling and Engineering Applications*, New York: Springer, 2008. https://doi.org/10.1007/978-0-387-47685-8
[28] M. Liu, J. Xu, and Q. Li, "Design and experiment of piezoelectric-shape memory alloy composite shock absorber," *Materials Letters*, vol. 304, 130538, 2021. doi: 10.1016/j.matlet.2021.130538
[29] J. W. Sohn, J. S. Ruth, D. G. Yuk, and S. B. Choi, "Application of shape memory alloy actuators to vibration and motion control of structural systems: A review," *Applied Sciences*, vol. 13, no. 2, 995, 2023. doi: 10.3390/app13020995
[30] A. Al-Falahat, "Analysis and modelling of the rotor dynamics of a composite hollow shaft using finite element techniques," *International Journal of Advanced Technology and Engineering Exploration*, vol. 10, no. 101, pp. 485–497, 2023. doi: 10.19101/IJATEE.2023.1010123
[31] A. M. Al-Falahat, "Examination of the dynamic behaviour of the composite hollow shafts subject to unbalance," *International Journal of Mechanical Engineering and Robotics Research*, vol. 10, no. 10, pp. 572–576, 2021. doi: 10.18178/ijmerr.10.10.572-576
[32] A. M. Al-Falahat, "Implementation of the dynamic balancing approach of a rotating composite hollow shaft," *EUREKA: Physics and Engineering*, no. 2, pp. 68–73, 2022. doi: 10.21303/2461-4262.2022.002231
[33] A. M. Al-Falahat, "The influence of silicon carbide on A356 aluminium alloy composites: Mechanical properties, thermal performance, Fourier transform infrared spectroscopy, corrosion resistance, and microstructural analysis," *Discover Applied Sciences*, vol. 7, no. 10, 2025. doi: 10.1007/s42452-025-0567-x
[34] A. Al-Falahat, "Metallurgical indices for physics-informed machine learning-based fatigue strength prediction in steels," *Journal of Failure Analysis and Prevention*, 2026. doi: 10.1007/s11668-026-01234-y